



TECHNICAL ARTICLE

Fracture Toughness of 22K-Type Low-Carbon Steel After Extreme Thermal Exposure

S.A. Nikulin, S.O. Rogachev, V.A. Belov, D.Yu. Ozherelkov, N.V. Shplis, L.V. Fedorenko, A.V. Molyarov, and K.A. Konovalova

Submitted: 17 December 2021 / Revised: 3 September 2022 / Accepted: 2 December 2022 / Published online: 15 December 2022

A complex of comparative studies on static fracture toughness according to the three-point bending scheme was carried out for the 22K low-carbon steel (AISI 1022) after various heat treatment, namely after normalization, after prolonged heat treatment provoking temper brittleness (TO-1 regime included heating to 650 °C and slow stepwise cooling for 7 days), and after high-temperature heat treatment causing intensive grain growth (TO-2 regime included heating to 1200 °C with holding for 3.7 h). The criterion of non-linear fracture mechanics, namely the critical J -integral taking into account plastic deformation at the crack tip was used as a characteristic of fracture toughness. It is shown that, regardless of the type of structure formed by different heat treatment, the 22K steel is characterized by high fracture toughness. However, after heat treatment by the TO-1 and TO-2 regimes, the value of the critical J -integral decreases by 23 and 30%, respectively.

Keywords fracture toughness, fracture, J -integral, low-carbon steels, microstructure

1. Introduction

Low-carbon steels such as 22K type (AISI 1022) are a widespread structural material in civil and industrial building (Ref 1-4). This is due to a good combination of their mechanical properties, namely satisfactory strength, high ductility, high impact and fracture toughness, as well as the low cost of these steels.

The 22K steel, in particular, is used for the manufacture of casings for core catcher vessel (CC-vessel), which ensure the safety of VVER nuclear reactors in a severe accident with a loss of coolant (Ref 5). In such accidents, the casing of the CC-vessel will be simultaneously exposed to prolonged high-temperature thermal impact and high static loads (Ref 6, 7).

Prolonged thermal exposure can significantly change the structure of the steel and, as a consequence, cause degradation of the mechanical properties of the CC-vessel material, which will lead to a loss of strength and an increase in the risk of failure (Ref 8, 9). To ensure the reliability of the CC-vessel under severe accidents at nuclear power plants, it is important to provide an optimal combination of strength and fracture toughness of the CC-vessel material, as the main parameter characterizing the metal's ability to resist the fracture process.

S.A. Nikulin, V.A. Belov, D. Yu. Ozherelkov, N.V. Shplis, L.V. Fedorenko, and K.A. Konovalova, National University of Science and Technology MISIS, Moscow, Russia; S.O. Rogachev, National University of Science and Technology MISIS, Moscow, Russia; and Baikov Institute of Metallurgy and Materials Science, Russian Academy of Sciences, Moscow, Russia; and A.V. Molyarov, Research and Development Center TMK (TMK R&D), Moscow, Russia. Contact e-mail: csaap@mail.ru.

There are few data in the literature on the fracture toughness (crack resistance) of low-carbon steels after prolonged (extreme) thermal exposure. One of the reasons is the difficulty in assessing the fracture toughness of highly ductile materials, which include low-carbon steels.

In this work, the comparative studies on the fracture toughness according to the three-point bending scheme of the 22K low-carbon steel with different structure after prolonged extreme thermal exposure were carried out.

2. Materials and Research Methods

Low-carbon steel grade 22K (ASTM grade 1022) as-delivered (60-mm thick sheet after hot rolling and normalization) was used as a starting material for the study. The chemical composition of the steel is shown in Table 1. The chemical composition of steel corresponded to GOST 5520-2017 (Russian document).

The fracture toughness tests of the 22K steel were carried out in three states:

1. As-delivered;
2. After heat treatment provoking temper brittleness, according to the TO-1 regime: heating up to 650 °C at a rate of 200 °C/h; cooling to 480 °C at a rate of 1 °C/h; further slow cooling in the furnace to room temperature (the total processing time was 7 days);
3. After heat treatment causing intensive grain growth, according to the TO-2 regime: heating up to 1200 °C at a rate of 200 °C/h; exposure 3.7 h; further slow cooling in the furnace to room temperature.

These regimes (TO-1 and TO-2) were obtained from results of computer simulation of the process cooling of the material of the nuclear reactor vessel during a severe accident (Ref 10, 11).

Table 1 The chemical composition of the 22K steel

Mass fraction of a chemical element, %										
Fe	C	Si	Mn	P	S	Cr	Ni	Cu	Mo	V
Bal	0.24	0.26	0.75	0.013	0.001	0.04	0.03	0.05	< 0.01	< 0.005

Heat treatment of the samples was carried out in an electric furnace of the SNVE 1.3.1/1614 type in a vacuum of $\sim 6.5 \times 10^{-3}$ Pa. To record temperature data in the course of heat treatment, an automatic digital recording of signals from control thermocouples was carried out.

The 22K steel is a material of medium strength and high ductility, which does not allow the use of the K_{1C} fracture toughness parameter as a characteristic of fracture toughness. Therefore, the parameter of non-linear fracture mechanics, so-called the critical J -integral (J_C) was chosen as a characteristic of fracture toughness (Ref 12). The critical J -integral characterizes the energy in the crack tip area, normalized to the unit displacement of the crack dl .

For comparative fracture toughness tests according to the static three-point bending scheme, flat rectangular notched T - S specimens were used (where T is the long transverse direction and S is the short transverse direction). The dimensions of the specimen were: height $b = 10.0 \pm 0.1$ mm, thickness $t = 5.0 \pm 0.1$ mm, length $L_1 = 55.0 \pm 0.1$ mm, and distance between supports $L = 50.0 \pm 0.1$ mm.

To determine the J -integral when testing notched specimens, we used the Begley–Landes experimental technique (Ref 13). In accordance with the technique, the fracture toughness of materials is estimated under elastoplastic conditions, when the intensity of deformation energy release during crack propagation is calculated as the fracture energy of the material spent per unit of crack length.

The value of the J -integral according to the Begley-Landes method for each selected deflection f is determined taking into account the specimen thickness t according to the Eq 1:

$$J = -(1/t) \times (dA/dl) \quad (\text{Eq 1})$$

where dA is the work of deformation before the crack starts, dl is the change in the crack length.

The test specimens were cut using a Chmer GX-360L CNC electric spark cutting machine. The surface of the specimens was ground with abrasive paper. Then, the notches were made on the specimens with a depth and width of 1.5 and 0.5 mm, respectively (Fig. 1). A sharp crack-like stress concentrator with a depth of $l = 1, 2, 3,$ and 4 mm and a width of $a = 0.1$ mm was made at the notch tip using a portable electric spark cutting machine with a wire diameter of 0.05 mm. Thus, the total depth of notch with stress concentrator h varied from 2.5 to 5.5 mm.

The fracture toughness tests were carried out at room temperature using an Instron 5569 universal testing machine. The load–deflection (P – f) curves and acoustic emission diagrams (AE-diagrams) coincided with time stamps were recorded in real test time.

There are various methods for determining the J_C -integral, namely by the maximum load on the P – f curve (Ref 14, 15); by changing in the slope of the linear section of the P – f curve

during unloading by 10-15% (Ref 16), etc. In this work, the critical load P_C when the crack starts at the notch tip, and the corresponding deflection f_C were determined by two methods:

- (1) By the AE signals using a special installation for recording AE (Ref 12, 16-18);
- (2) By the direct observation on the lateral surface of the specimen from the analysis of the stress and strain fields at the notch tip.

AE registration was carried out using a setup based on a PXI-1042Q modular measuring platform with a built-in NI PXI-5152 ADC board, an amplifier, and a piezoceramic sensor directly recording the AE signals (Ref 16). The sensor was fixed on the polished surface of the specimen end part through a thin layer of glycerin and connected to the AE measuring module. The average level of technological noise of the equipment was about 10 mV. Taking into account a 12-bit analog-to-digital converter and the dynamic range of 4 V, the noise threshold was set equal to 90-100 mV. Therefore, we took into account AE signals with an amplitude above 100 mV.

The data for plotting the stress and strain fields at the notch tip have been recorded using a special digital optical system. For this, a speckled pattern was painted on the specimen surface. Video files were processed using the GOM Correlate program used a digital image correlation (DIC) technique.

To calculate the J -integral parameter, the P – f curve in the range from 0 to f_C was approximated polynomially (the coefficient of determination $R^2 \geq 0.97$) to obtain the equation of the function $P(f)$. The work of deformation A was determined as the area under the P – f curve by integrating the P – f curves using the Origin 2019 mathematical package. The result was used to plotting the A – f calibration curves for the notches of different depths.

To determine the value of the fracture toughness parameter J_C , the J – f calibration dependence was plotted, which was then approximated by the linear function $Y = kX + b$ and, using Eq 1, the value $J = -k$ [J/m²] was calculated, where Y is the work normalized to the crack propagation path value [J/m], X is the depth of the crack-like stress concentrator (0.001-0.004 m), k is the mechanical energy expended per unit of the crack length, normalized to the specimen thickness ($t = 0.005$ m). The J_C values were determined by the deflection f_C on the J – f calibration curves when the crack starts.

The analysis of the fractures of the specimens after their breaking was carried out using a JSM-IT500 (JEOL) scanning electron microscope at a magnification of $\times 20$ -1500. The fracture surfaces were imaged for the area under the notch tip. The quantitative analysis of the specimens' fractures (the fraction of the brittle component in the fracture) was carried out using the Image Expert Pro 3 software environment.

The microstructure of the 22K steel was studied using an AxioObserver D1m CarlZeiss optical microscope at a magni-

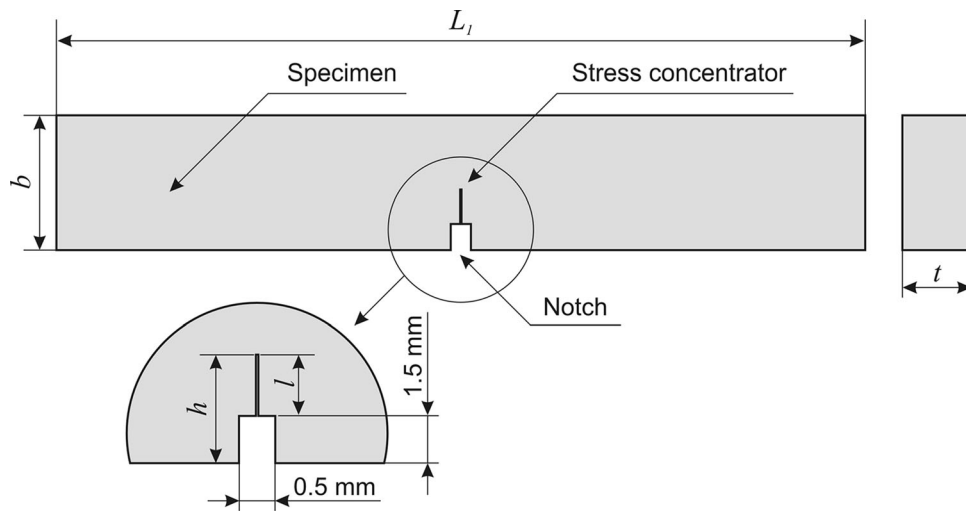


Fig. 1 Schematic image of a fracture toughness test specimen

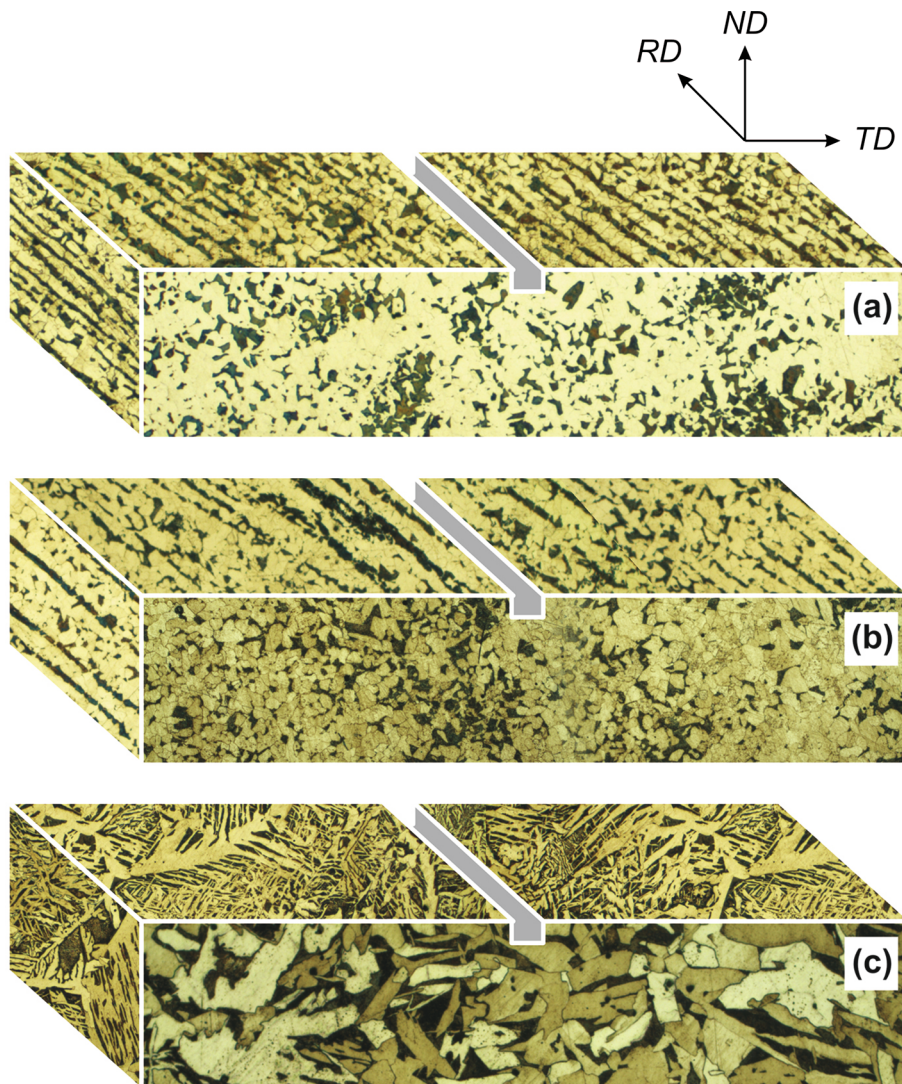


Fig. 2 Schematic image of the microstructure of the 22K steel specimens: (a) as-delivered; (b) TO-1; (c) TO-2

fication of $\times 200$ after etching the sections using a nitric acid 5% (v/v) in aqueous solution.

3. Results and Discussion

Figure 2 shows the schematic images of the microstructure in different sections of the 22K steel specimens after various heat treatments. The as-delivered steel is characterized by ferrite-pearlite banding in the direction of rolling (RD) (Fig. 2a). After heat treatment by the TO-1 regime, ferrite-pearlite banding in the steel structure is preserved (Fig. 2b). On the contrary, after heat treatment by the TO-2 regime, a coarse-

grained structure with an internal acicular structure (Widmanstätten) is formed, which is typical for overheated steel (Fig. 2c). The microstructure is shown in more detail in Fig. 3. As-delivered state, the average grain sizes of ferrite and pearlite were 18 ± 2 and $13 \pm 4 \mu\text{m}$, respectively. After heat treatment by the TO-1 regime, the average grain sizes of ferrite and pearlite were 25 ± 2 and $16 \pm 2 \mu\text{m}$. After heat treatment by the TO-2 regime, the grain size was $558 \pm 210 \mu\text{m}$; in this case, a strong uneven grain-size distribution was observed.

The examples of combined P - f curves and AE diagrams for the 22K steel specimens after various heat treatments, obtained during bending tests, are shown in Fig. 4, and the values of the mechanical properties are in Table 2.

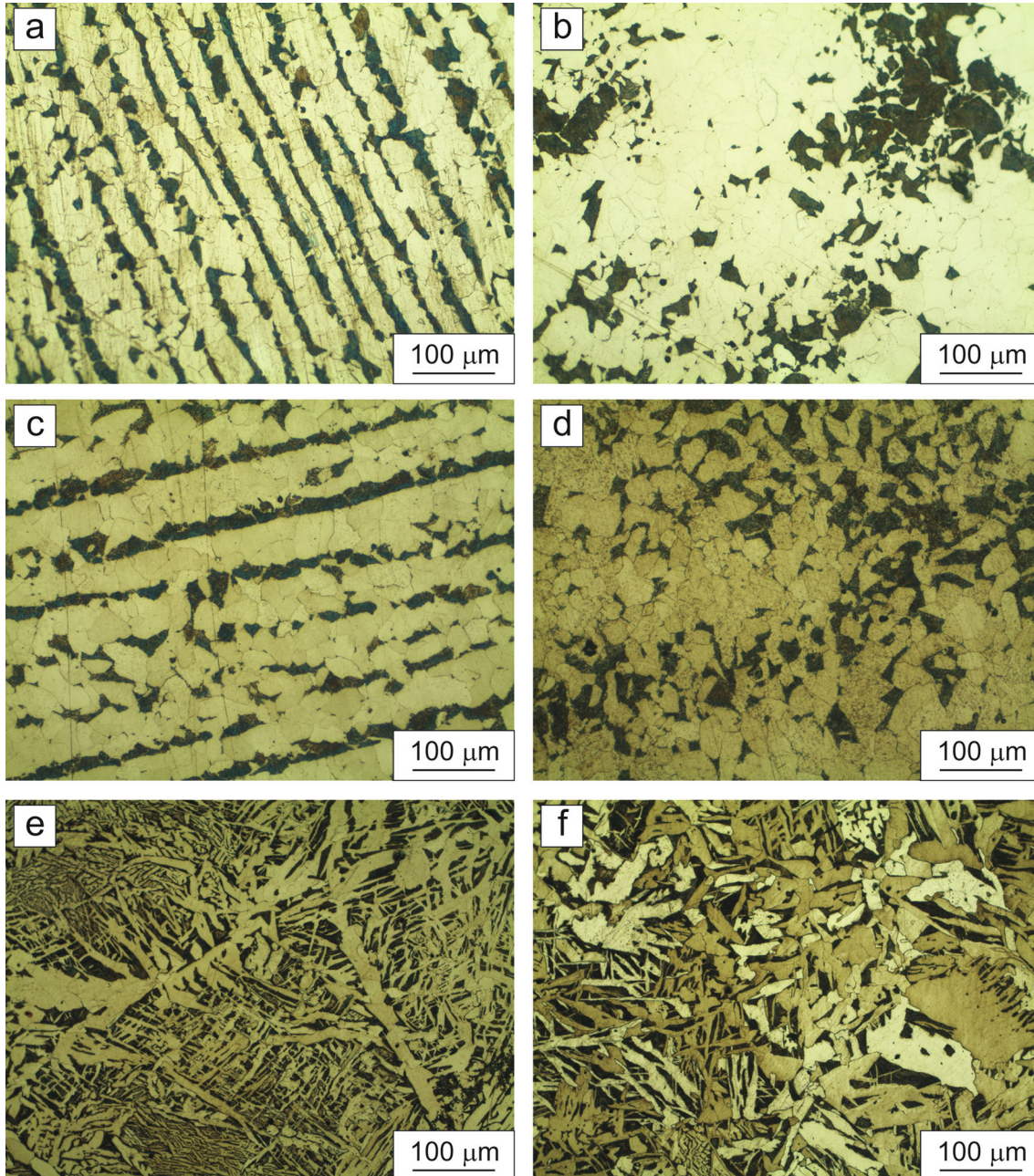


Fig. 3 Microstructure of the 22K steel sheet in longitudinal (a, c, e) and transverse (b, d, f) directions: (a, b) as-delivered; (c, d) TO-1; (e, f) TO-2

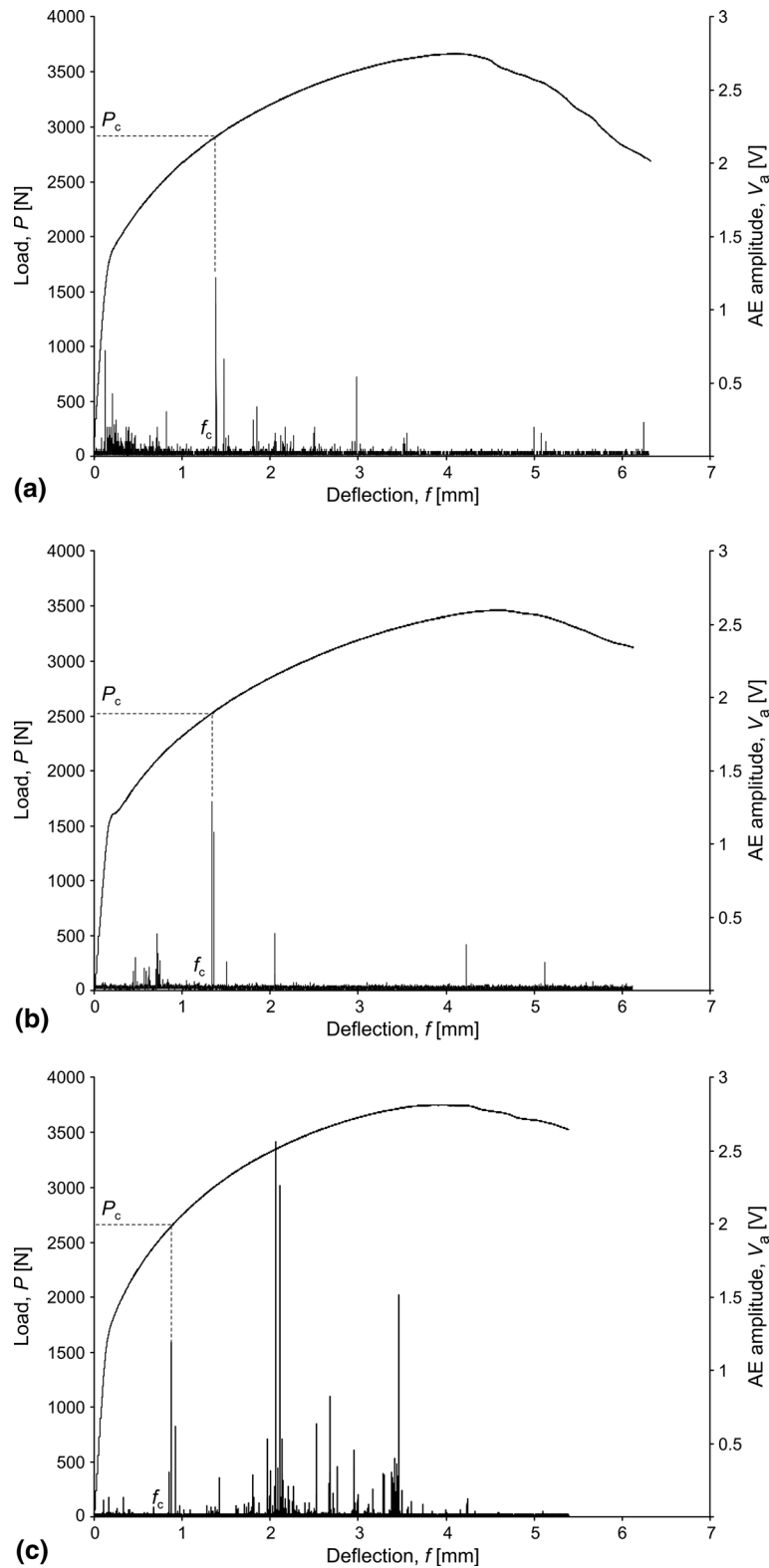


Fig. 4 Examples of combined P - f -curves and AE diagrams when testing the 22K steel specimens with a 1-mm depth stress concentrator after various heat treatments: (a) as-delivered; (b) TO-1; (c) TO-2 (the arrow shows the moment of the crack start)

The visualization of the stress-strain state at the notch tip of the specimens under loading is shown in Fig. 5, 6 and 7. When the specimens were loaded above the yield point, a stress concentration area was observed at the notch tip (Fig. 5a, 6a and 7a). Then the crack started and opened, which corre-

sponded to a deflection of 0.8-1.5 mm (depending both on the steel structure and the stress concentrator depth) (Fig. 5b, 6b and 7b). This moment was accompanied by the appearance of the first AE signal with large amplitude (over 1 V) (Fig. 4). Thus, the moment of the crack start, determined by direct

Table 2 Characteristics of static fracture toughness of the 22K steel after various heat treatments

Stress concentrator depth, mm	Maximum load, P_{\max} , N	$P_{\max}/(b-h)$, N/mm	Critical deflection, f_c , mm	Critical load, P_c , N
<i>As-delivered (after normalization)</i>				
1	3629 ± 68	484 ± 9	1.38 ± 0.03	2882 ± 41
2	2803 ± 58	431 ± 9	1.47 ± 0.03	2365 ± 27
3	2082 ± 45	378 ± 8	1.41 ± 0.03	1638 ± 37
4	1577 ± 5	350 ± 1	1.43 ± 0.02	1385 ± 18
<i>TO-1</i>				
1	3497 ± 110	466 ± 15	1.24 ± 0.02	2482 ± 26
2	2722 ± 7	419 ± 1	1.24 ± 0.02	1974 ± 28
3	1920 ± 22	349 ± 4	1.12 ± 0.03	1628 ± 22
4	1381 ± 4	307 ± 1	1.29 ± 0.02	984 ± 20
<i>TO-2</i>				
1	3700 ± 85	493 ± 11	0.88 ± 0.02	2678 ± 39
2	2864 ± 47	441 ± 7	1.11 ± 0.02	2089 ± 24
3	1960 ± 16	356 ± 3	0.78 ± 0.02	1350 ± 21
4	1480 ± 9	329 ± 2	0.83 ± 0.02	997 ± 28

observation on the lateral surface of the specimen, coincides with the moment of registration of a large-amplitude AE signal. With further loading at the uniform plastic deformation stage, the crack front went along two symmetrical directions oriented at an angle close to 45° in both directions from the notch (Fig. 5c, 6c and 7c). Further crack propagation was accompanied by a drop in the load on the P - f curve and several AE signals with large amplitude from 0.3 to 2.5 V. Thus, the start of the crack and its propagation did not lead to the final failure of all specimens during testing.

The A - f calibration dependences for steel after various heat treatments are shown in Fig. 8. As noted above, in this work, to determine the J_C -integral value, the moment of the crack start was experimentally recorded. The performed calculation showed that the J_C value for as-delivered steel was 120 ± 2 kJ/m². After heat treatment by the TO-1 regime provoking temper brittleness, the J_C value was 92 ± 9 kJ/m², i.e. heat treatment by the TO-1 regime decreased the fracture toughness value of the 22K steel by 23%. After heat treatment by the TO-2 regime causing intensive grain growth, the J_C value was 81 ± 14 kJ/m², i.e. heat treatment by the TO-2 regime decreased the fracture toughness of the 22K steel by 30%; in this case, the spread of J_C values increases.

With an increase in the stress concentrator depth from 1 to 4 mm, the maximum load (P_{\max}) on the P - f curve decreases for steel specimens of all states (Table 2). In this case, for the specimens with short stress concentrators (1-2 mm), the P_{\max} value after heat treatment by the TO-1 regime does not significantly differ from the P_{\max} value for the as-delivered steel; and for the long stress concentrators (3-4 mm), the P_{\max} value after heat treatment by the TO-1 regime is decreased by 8-12%. After heat treatment by the TO-2 regime, the P_{\max} value for all stress concentrator depths does not significantly differ from the P_{\max} value for the as-delivered steel. The ratio of the maximum load P_{\max} to the specimen height without taking into account the total depth of notch with stress concentrator (b minus h) for the steel specimens of all states depends on the stress concentrator depth, namely decreases by 28-34% with an increase in the stress concentrator depth from 1 to 4 mm. This circumstance confirms the sensitivity of the test to the stress concentrator depth.

The fractures of the 22K steel specimens in all states have a similar macrostructure. In the area under the notch tip, an area of the crack opening is visible, which has a characteristic parabolic shape (Fig. 9a, 10a and 11a). Further, an area of stable crack propagation is observed, which turns into a final rupture. The fracture of the specimen in the area of the crack opening under the notch tip occurs according to a mixed mechanism: there are both areas of ductile dimple fracture and areas of brittle fracture, represented by quasi-cleavage facets (Fig. 9b, 10b, and 11b). The fraction of quasi-cleavage in fractures (in the area of the crack opening) of the as-delivered specimens is 15-16% (Fig. 12). This is comparable to the fraction of quasi-cleavage in the fractures (in the area of the crack opening) of the specimens after heat treatment by the TO-1 regime. After heat treatment by the TO-2 regime, the fraction of quasi-cleavage in fractures (in the area of the crack opening) increases to 25-36%, i.e. 1.7-2.4 times. An increase in the brittle component (and a simultaneous decrease in the J_C -integral value) in this case can be associated with the presence of an acicular structure, which sharply decreases the resistance of the metal to brittle fracture.

The shape and size of the area of the crack opening did not depend on the stress concentrator depth. For as-delivered steel and for steel after heat treatment by the TO-1 regime, the size of the crack opening area is comparable, and for steel after heat treatment by the TO-2 regime, it is ~ 2 times larger. In this case, the predominantly ductility dimple mechanism of final rupture in as-delivered steel specimen is replaced by a cleavage and quasi-cleavage brittle mechanism in the specimens after heat treatment by the TO-1 regime; and by a cleavage brittle mechanism in the specimens after heat treatment by the TO-2 regime.

It is important to note that the fracture toughness characteristics of the 22K steel turned out to be less sensitive to changes in the structure of the specimens caused by prolonged thermal exposure than the impact toughness characteristics. Thus, in previous works, when studying the 22K steel specimens after heat treatment according to a regime similar to TO-1, a significant increase in the temperature of the ductile-brittle transition by 30-40 °C (from room temperature to 50-60 °C) was observed (Ref 9). A more significant degradation of impact toughness was observed for the 22K steel specimens

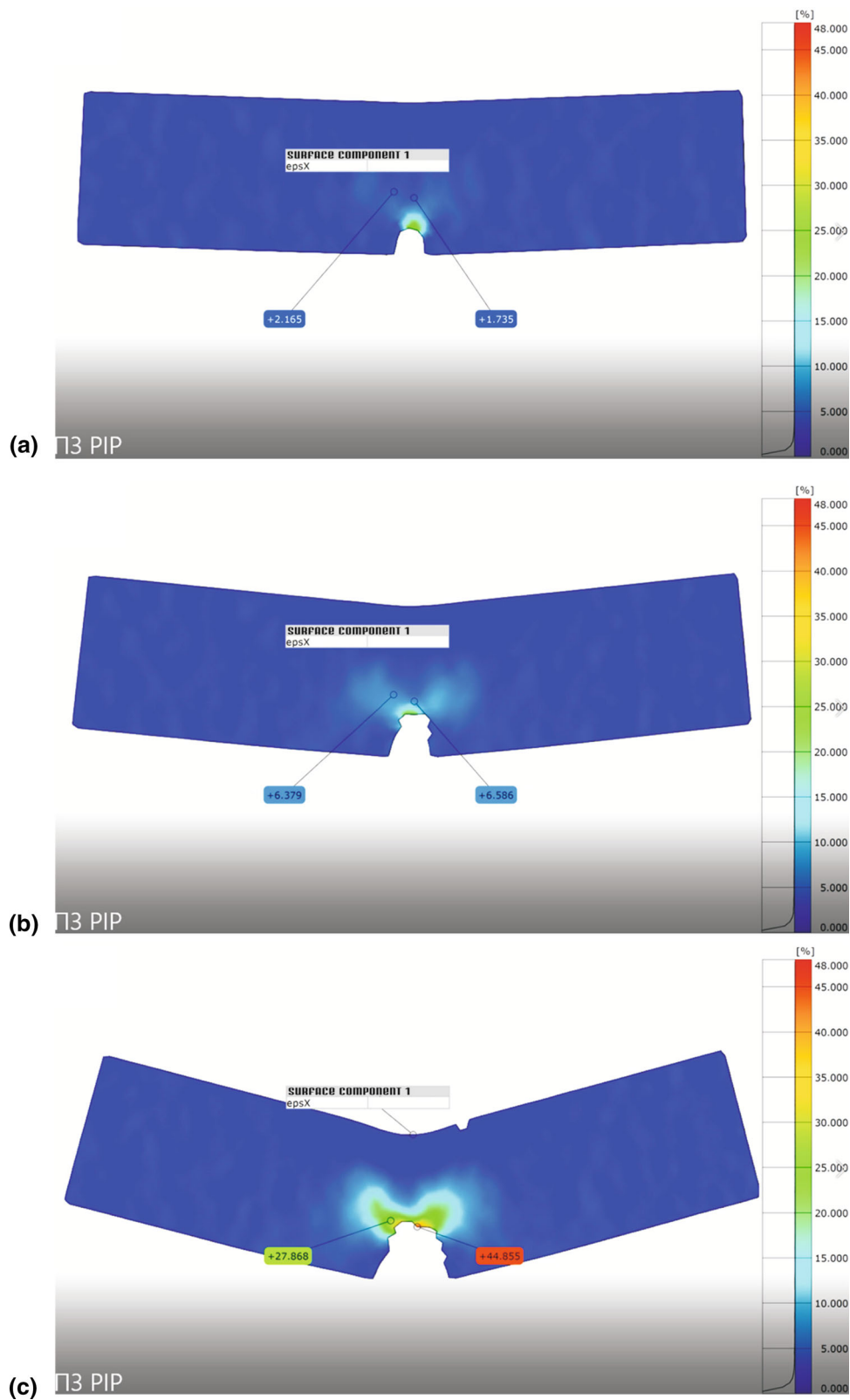


Fig. 5 Development of the stress–strain state during bending loading of the 22K steel specimen with a 1-mm depth stress concentrator in the as-delivered state: (a) the deformation field before the crack starts; (b) the deformation field during the crack opening; (c) stress concentration at the tip of propagate cracks

with a coarse-grained structure after prolonged high-temperature exposure. For example, heating to a temperature of 1000 °C (which is 200 °C lower than the maximum temper-

ature of heat treatment by the TO-2 regime) followed by very slow cooling led to an increase in the temperature of the

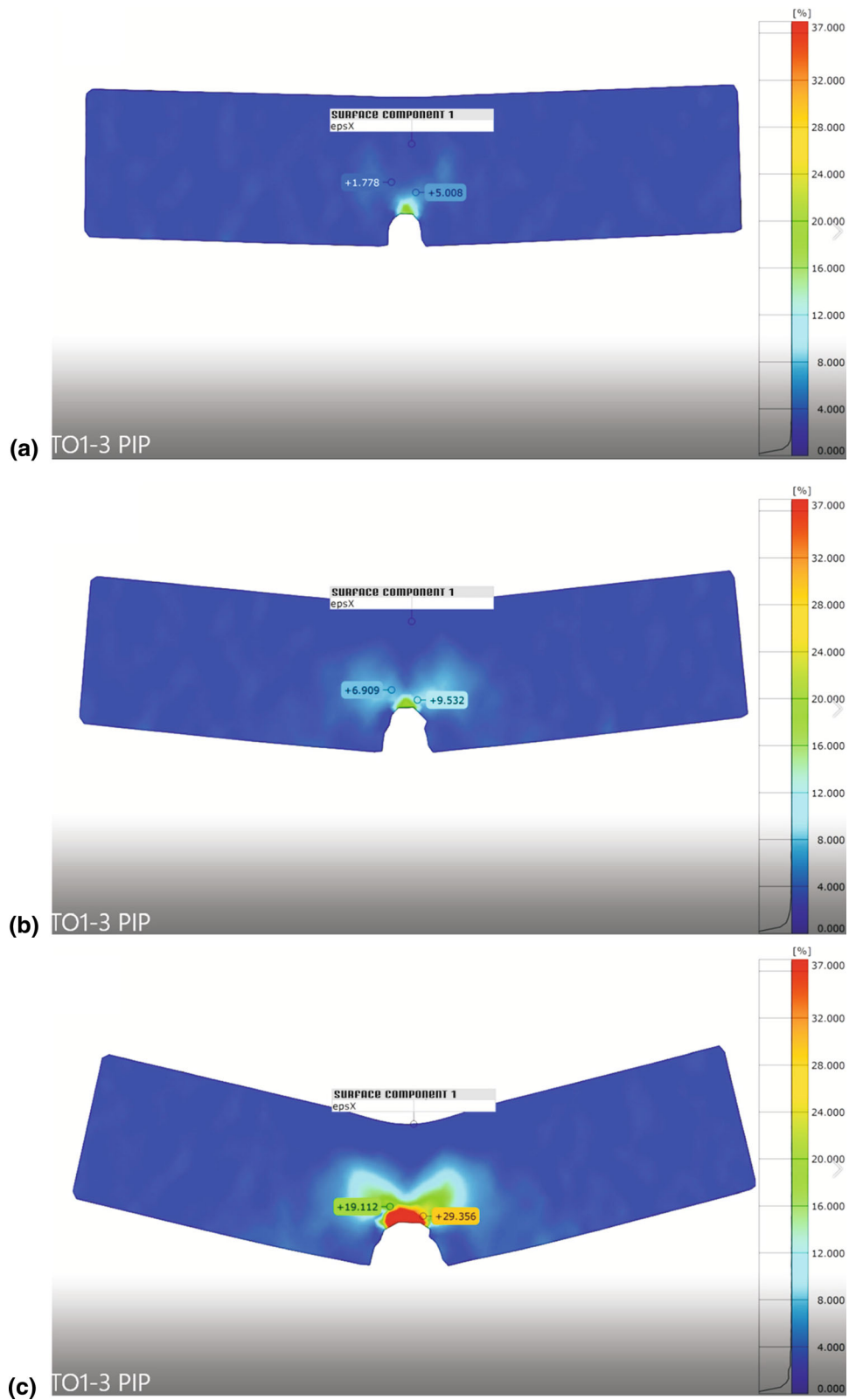


Fig. 6 Development of the stress–strain state during bending loading of the 22K steel specimen with a 1-mm depth stress concentrator after TO-1: (a) the deformation field before the crack starts; (b) the deformation field during the crack opening; (c) stress concentration at the tip of propagate cracks

ductile–brittle transition by 40–55 °C (from room temperature to 75 °C) (Ref 10).

Thus, the prolonged thermal exposure in the temperature range of temper brittleness had a negative effect on static fracture toughness. However, in spite of the decrease in the J_C -

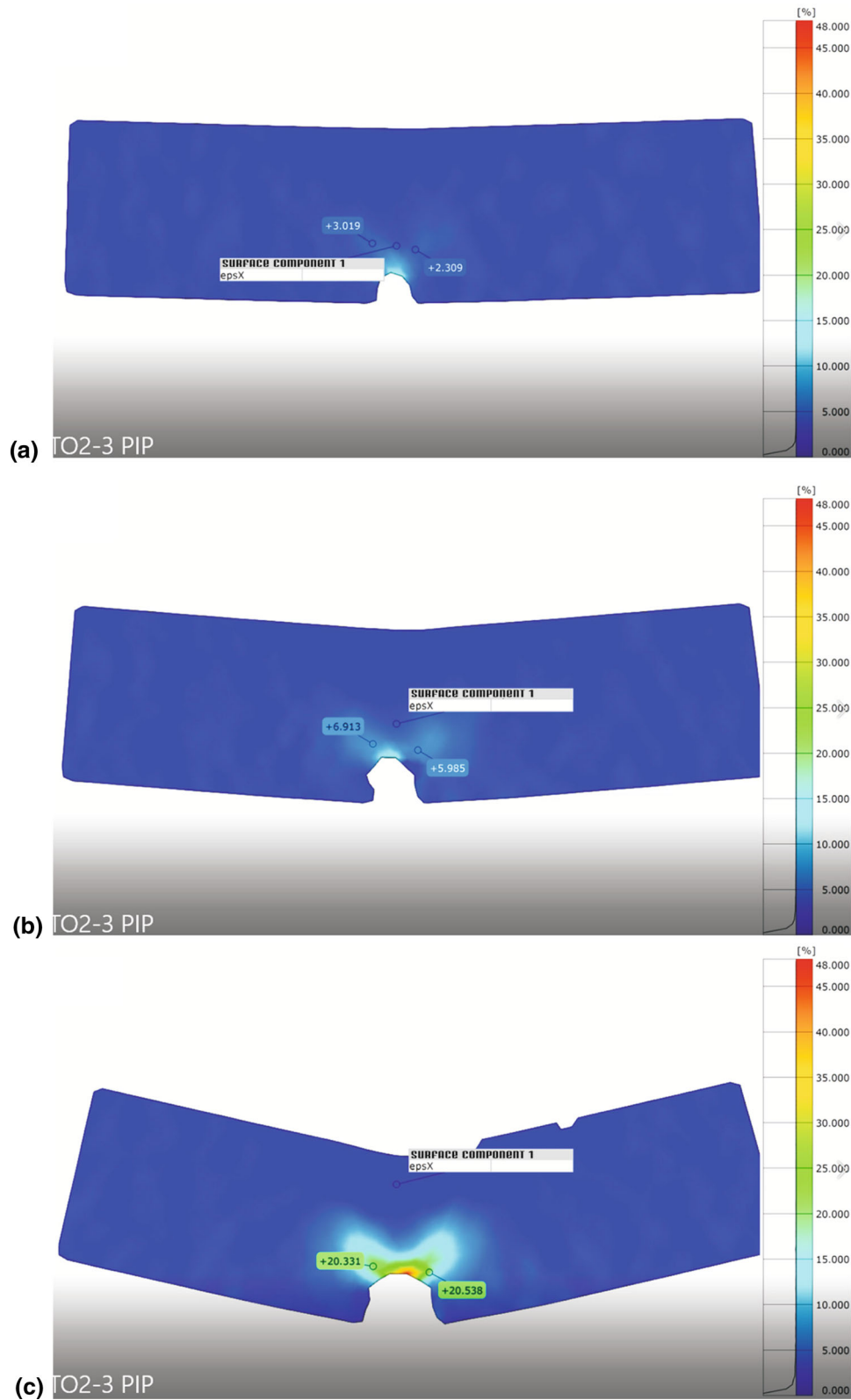


Fig. 7 Development of the stress–strain state during bending loading of the 22K steel specimen with a 1-mm depth stress concentrator after TO-2: (a) the deformation field before the crack starts; (b) the deformation field during the crack opening; (c) stress concentration at the tip of propagate cracks

integral value after thermal exposure, the steel in all states had high fracture toughness, and for all tested specimens, the crack opening did not lead to catastrophic brittle fracture. The

strongest decrease in the J_C -integral value (by 30%) was observed for steel with a coarse-grained structure as well as the

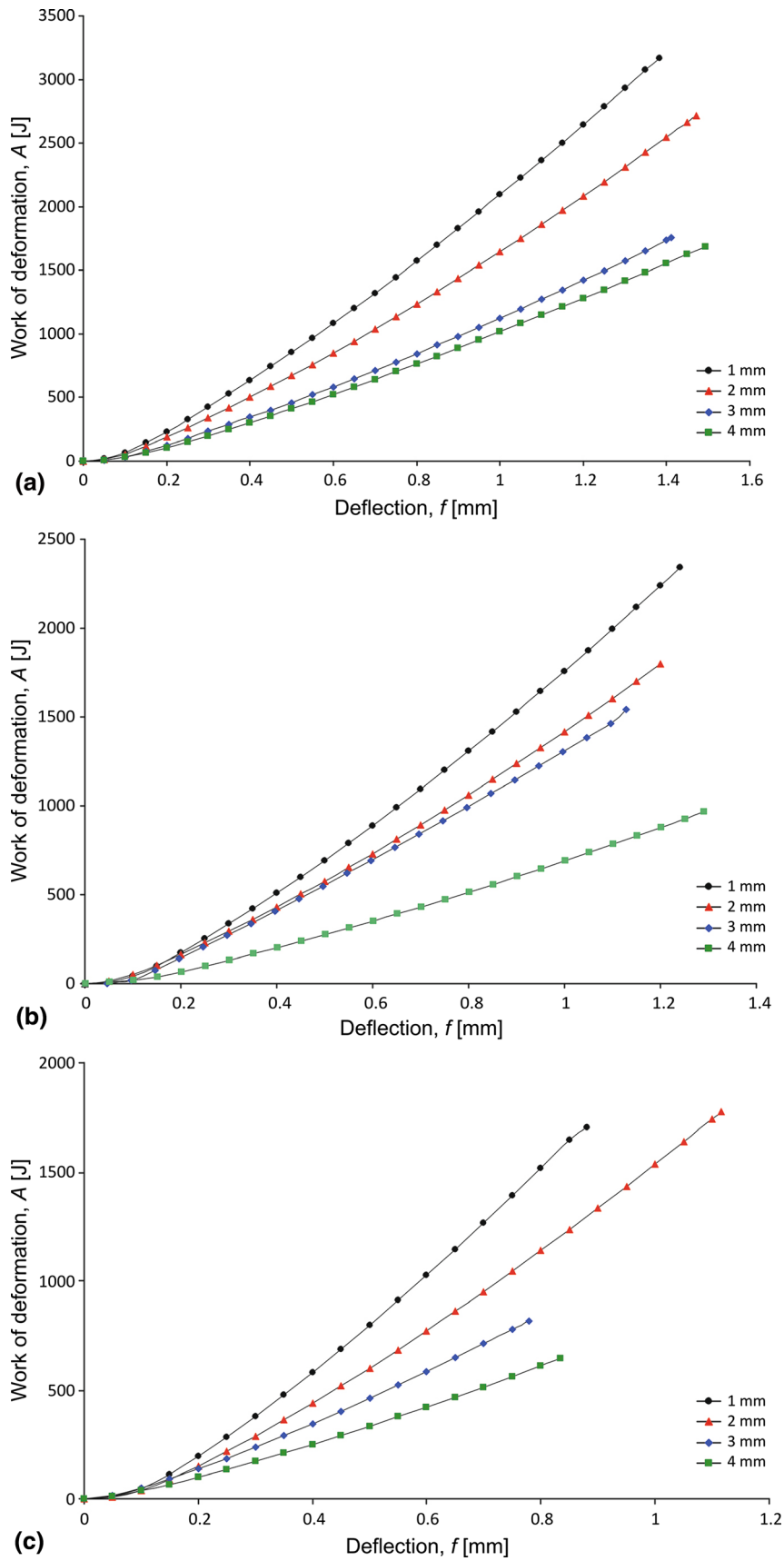


Fig. 8 A - f calibration curves for the specimens with stress concentrator depth from 1 to 4 mm: (a) as-delivered; (b) TO-1; (c) TO-2

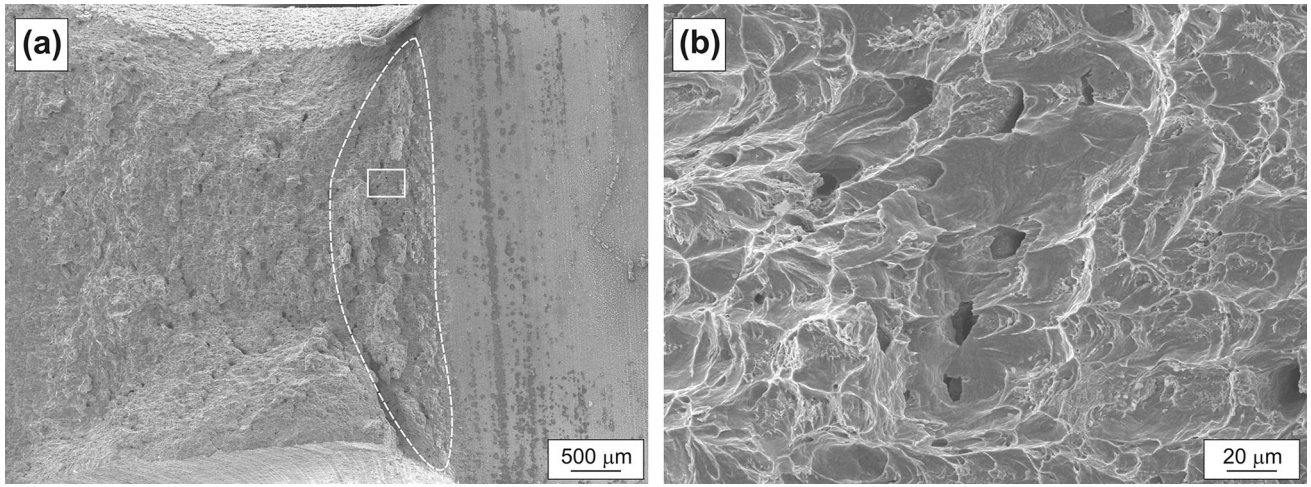


Fig. 9 Fracture surface of the 22K steel specimen with a 4-mm depth concentrator in as-delivered state after bending tests and breaking

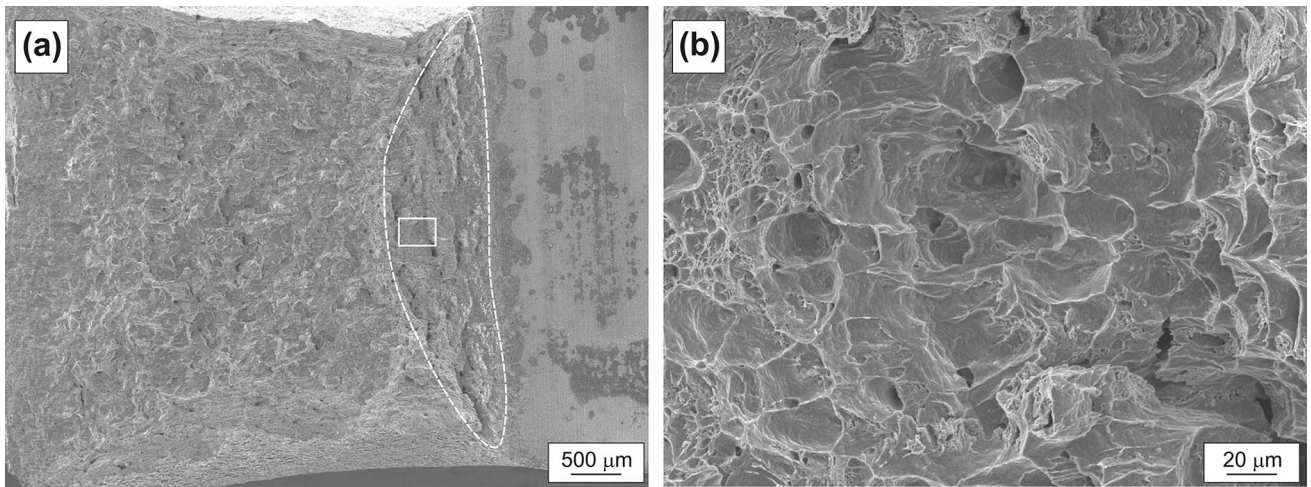


Fig. 10 Fracture surface of the 22K steel specimen with a 4-mm depth concentrator after heat treatment by the TO-1 regime and after bending tests and breaking

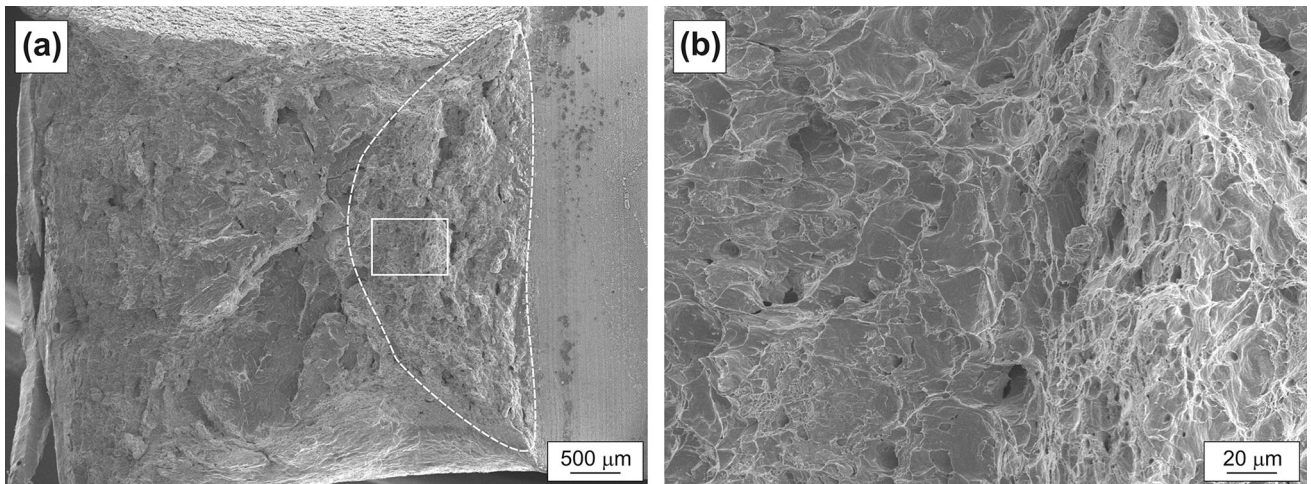


Fig. 11 Fracture surface of the 22K steel specimen with a 4-mm depth concentrator after heat treatment by the TO-2 regime and after bending tests and breaking

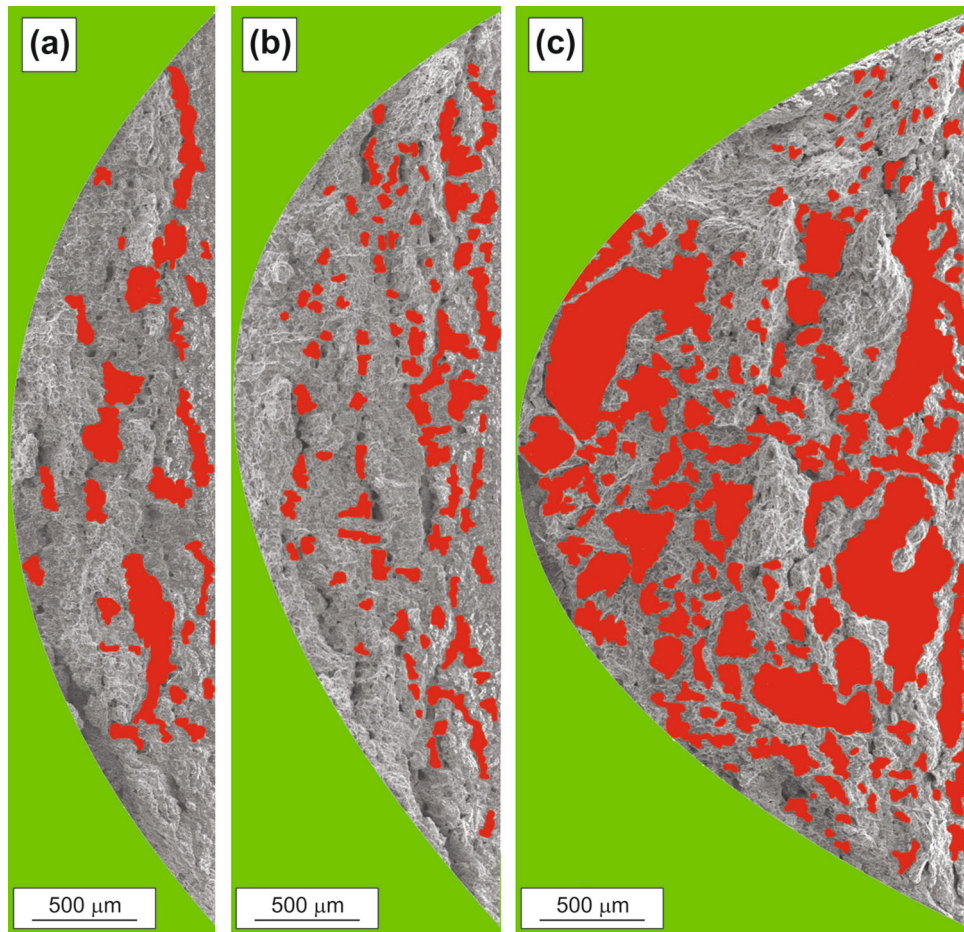


Fig. 12 Area of crack opening in fractures of the 22K steel specimens with a 1-mm depth concentrator: (a) as-delivered; (b) TO-1; (c) TO-2 (the brittle component is highlighted in red)

increase (1.7-2.4 times) of the fraction of the brittle component in the fractures of the specimens.

4. Conclusions

Based on the results of a study for static fracture toughness according to the bending scheme of the 22K low-carbon steel after various heat treatments, it was established:

- (1) As-delivered steel (hot rolling + normalization) with ferrite-pearlite banding in the direction of rolling is characterized by high fracture toughness with a value of $J_C = 118-122 \text{ kJ/m}^2$;
- (2) After prolonged thermal exposure in the temper brittle temperature range, steel retains ferrite-pearlite banding, while the J_C value decreases compared with the as-delivered state (by an average of 23%) and is $78-99 \text{ kJ/m}^2$, and the fraction of the brittle component in fractures of specimens (15-16%) is comparable to the fraction of the brittle component in fractures of the as-delivered specimens;
- (3) After prolonged thermal exposure in the temperature range of intensive grain growth, steel is characterized by a coarse-grained structure of the “Widmanstätt” type, while the J_C value decreases by an average of 30%

compared with the as-delivered state and is $67-101 \text{ kJ/m}^2$, and the fraction of the brittle component in fractures of specimens increases 1.7-2.4 times;

- (4) For all tested specimens, the crack opening did not lead to their catastrophic brittle fracture.

Acknowledgments

The study of the structure was carried out using the equipment of the Center for Collective Use ‘Materials Science and Metallurgy’ with the financial support of the Ministry of Science and Higher Education of the Russian Federation (#075-15-2021-696).

References

1. R.G. Budynas and J.K. Nisbett, *Shigley’s Mechanical Engineering Design*, 9th ed. McGraw-Hill, New York, 2011
2. P.D. Odesskii and A.A. Egorova, Strength of Steel for Unique Engineering Structures, *Russ. Metall.*, 2012, **2012**(10), p 911. <https://doi.org/10.1134/S0036029512100151>
3. C.-C. Yang and C.-L. Liu, Improvement of the Mechanical Properties of 1022 Carbon Steel Coil by Using the Taguchi Method to Optimize Spheroidized Annealing Conditions, *Materials*, 2016, **9**, p 693. <http://doi.org/10.3390/ma9080693>
4. V.S. Belkin, P.N. Belkin, B.L. Krit, N.V. Morozova, and S.A. Silkin, Increasing Wear Resistance of Low-Carbon Steel by Anodic Plasma-

- Electrolytic Nitroboriding, *J. Mater. Eng. Perform.*, 2000, **29**, p 564. <https://doi.org/10.1007/s11665-019-04521-1>
5. J.L. Rempe, D.L. Knudson, K.G. Condie, K.Y. Suh, F.-B. Cheung, and S.-B. Kim, Conceptual Design of an In-Vessel Core Catcher, *Nucl. Eng. Des.*, 2004, **230**, p 311. <https://doi.org/10.1016/j.nucengdes.2003.11.030>
 6. M. Fischer, The Severe Accident Mitigation Concept and the Design Measures for Core Melt Retention of the European Pressurized Reactor (EPR), *Nucl. Eng. Des.*, 2004, **230**, p 169.
 7. T. Sultan, M.K. Sapra, S. Kundu, A.V. Kadam, P.P. Kulkarni, and A.R. Rao, Experimental & Analytical Study of Passive Thermal Sensing System Developed for Cooling Water Injection into AHWR Core Catcher, *Nucl. Eng. Des.*, 2017, **322**, p 81. <https://doi.org/10.1016/j.nucengdes.2003.11.034>
 8. V. Loktionov, I. Lyubashevskaya, O. Sosnin, and E. Terentyev, Short-Term Strength Properties and Features of High-Temperature Deformation of VVER Reactor Pressure Vessel Steel 15Kh2NMFA-A Within the Temperature Range 20–1200 °C, *Nucl. Eng. Des.*, 2019, **352**, 110188. <https://doi.org/10.1016/j.nucengdes.2019.110188>
 9. S.A. Nikulin, S.O. Rogachev, S.G. Vasil'ev, V.A. Belov, and A.A. Komissarov, Effect of Long-Term Annealing on the Impact Toughness of 22K Steel, *Russ. Metall.*, 2021, **2021**(4), p 149. <https://doi.org/10.1134/S0036029521040248>
 10. S.A. Nikulin, S.O. Rogachev, V.A. Belov, A.A. Komissarov, VYu. Turilina, N.V. Shplis, and Yu.A. Nikolaev, Influence of Long-Term High-Temperature Action on the Impact Toughness of the Base Metal and the Weld Metal of the 22K Steel Welded Joint, *Steel Transl.*, 2021, **51**, p 428. <https://doi.org/10.3103/S0967091221070068>
 11. S.A. Nikulin, S.O. Rogachev, V.A. Belov, MYu. Zadorozhnyy, N.V. Shplis, and M.M. Skripalenko, Effect of Prolonged Thermal Exposure on Low-Cycle Bending Fatigue Resistance of Low-Carbon Steel, *Metals*, 2022, **12**, p 281. <https://doi.org/10.3390/met12020281>
 12. V.A. Belov, A.V. Nikitin, V.I. Anikeenko, A.A. Armizonov, and S.O. Rogachev, Fracture Toughness of As-Cast Freight Bogie Solebars after Volume-Surface Quenching, *Russ. Metall.*, 2017, **2017**(10), p 874. <https://doi.org/10.1134/S0036029517100032>
 13. J.A. Begley and J.D. Landes, *The J-integral as a fracture criterion*. In: Fracture Toughness, Part II, ASTM STP 514, 1972, pp 1–20
 14. T. Miyoshi and H. Miyata, Study on J_c Fracture Criterion. Evaluation of Fracture Toughness by J-Integral and COD Methods, *J. Fac. Eng. Univ. Tokyo*, 1975, **33**(2), p 186–190.
 15. G.A. Clarke, W.R. Andrews, P.C. Paris, and D.W. Schmidt, *Single specimen tests for J_C determination*. In: Mechanics of Crack Growth, ASTM STP 590, 1976, no 590, pp 27–42
 16. V.G. Khanzhin, Designing Computer Systems for Acoustic Emission Materials Testing, *Met. Sci. Heat Treat.*, 2009, **51**(5–6), p 245. <https://doi.org/10.1007/s11041-009-9161-5>
 17. A.A. Stepashkin, DYu. Ozherelkov, Yu.B. Sazonov, and A.A. Komissarov, Fracture Toughness Evolution of a Carbon/Carbon Composite After Low-Cycle Fatigue, *Eng. Fract. Mech.*, 2019, **206**, p 442. <https://doi.org/10.1016/j.engfracmech.2018.12.018>
 18. V.G. Khanzhin and M.A. Shtremel, Quantitative Information on Damage Processes Obtained in Acoustic Emission Measurements, *Met. Sci. Heat Treat.*, 2009, **51**(5–6), p 250. <https://doi.org/10.1007/s11041-009-9146-4>

Publisher's Note Springer Nature remains neutral with regard to jurisdictional claims in published maps and institutional affiliations.

Springer Nature or its licensor (e.g. a society or other partner) holds exclusive rights to this article under a publishing agreement with the author(s) or other rightsholder(s); author self-archiving of the accepted manuscript version of this article is solely governed by the terms of such publishing agreement and applicable law.